Broadband Millimeter-Wave Textile-Based Flexible Rectenna for Wearable Energy Harvesting

Mahmoud Wagih, *Student Member, IEEE*, Geoffrey S. Hilton, Alex S. Weddell, *Member, IEEE*, and Steve Beeby, *Senior Member, IEEE*

Abstract—Millimeter-Wave (mmWave) bands, a key part of future 5G networks, represent a potential channel for RF energy harvesting, where the high-gain antenna arrays offer improved end-to-end efficiency compared to sub-6 GHz networks. This paper presents a broadband mmWave rectenna, the first rectenna realized on a flexible textile substrate for wearable applications. The proposed novel antenna's bandwidth extends from 23 to 40 GHz, with a minimum radiation efficiency of 67% up to 30 GHz, over 3 dB improvement compared to a standard patch. A stable gain of more than 8 dB is achieved based on a textile reflector plane. The antenna is directly connected to a textile-based microstrip voltage doubler rectifier utilizing commercial Schottky diodes. The rectifier is matched to the antenna using a tapered line feed for high-impedance matching, achieving broadband high voltage-sensitivity. The rectifier has a peak RF-DC efficiency of 12% and a 9.5 dBm 1 V sensitivity from 23 to 24.25 GHz. The integrated rectenna is demonstrated with more than 1.3-V DC output from 12 dBm of mmWave wireless power across a 28% fractional bandwidth from 20 to 26.5 GHz, a 15% half-power fractional bandwidth, and a peak output of 6.5V from 20 dBm at 24 GHz.

Index Terms—Antennas, Broadband matching networks, Internet of Things, Microstrip antennas, Rectennas, Rectifier, RF Energy Harvesting, Wearable Antenna, Wireless Power Transfer

I. INTRODUCTION

MILLIMETER-WAVE (mmWave) bands will play a significant role in future 5G networks, where the broad spectrum aims to mitigate traffic-related issues in existing sub-6 GHz networks. Although mmWaves suffer from increased propagation losses due to absorption by air and water molecules around 20 and 60 GHz, respectively, the large number of channels, beamforming and high-gain large antenna arrays are attractive features of mmWave networks [1]. The low-cost, pervasive Internet of Things (IoT) market not only benefits from the wider spectrum allowing trillions of devices to communicate, but also from the potential of utilizing

mmWave bands to achieve power-autonomy through wireless energy harvesting.

Wireless Power Transfer (WPT) and Radio Frequency Energy Harvesting (RFEH) networks with Simultaneous Wireless Information and Power Transfer (SWIPT) at mmWave bands are expected to co-exist in future 5G networks [2], where a key research challenge is enabling wireless powering of Internet of Everything (IoE) networks as a fundamental component of 5G networks [3]. RFEH in a 28 GHz network has been investigated numerically demonstrating improved energy and information coverage over sub-6 GHz networks, promising improved end-to-end RFEH efficiency over existing cellular networks [4], [5]. The improvement in energy-coverage and hence end-to-end efficiency can be attributed to the beamforming techniques based on base-stations with large antenna arrays which can be realized in smaller areas, due to the antennas' reduced size. Moreover, area constrained applications such as single-chip active RFID transmitters benefit from mmWave WPT due to the higher achievable antenna efficiencies with sub-mm^2 aperture size [6].

Rectennas for WPT at mmWave frequencies have been previously presented, with focus on the 24 [7], [8] and 60 GHz license-free spectrum [9]. A circularly-polarized cavity-backed rectenna array [7], a Substrate-Integrated Waveguide (SIW) rectenna [10], as well as inkjet printed flexible rectennas on paper [11] and high-frequency Liquid Crystal Polymer (LCP) [12] have been reported. However, the rectennas have mostly been studied under single-tone excitation at 24 GHz. SIW structures have been used in mmWave rectennas due to their ability to improve the antennas' gain and isolation from surroundings, nevertheless, a SIW rectenna would normally target single bands and require an external microstrip matching network along with a SIW to microstrip transition, adding to the system's complexity [10]. Finally, while various antenna designs and matching architectures have been reported sub-6 GHz [13], mmWave rectennas have been mostly limited to patch arrays and SIW antennas.

In order to overcome the cost-barrier of mmWave rectennas fabricated on low-loss RF substrates, additive manufacturing has been used to realize mmWave rectennas for pervasive IoT [12], [14], [15]. While the reported additively manufactured rectennas achieve a 1-V output from as low as 10 dBm of mmWave power, they were all studied under single-tone excitation and are expected to have their bandwidth bottle-necked due to the use of patch antennas and narrow-band beamforming or array-feed networks. Therefore, their ability to be extended to harvest power from the full 5G commercial

spectrum is limited.

Although most low power mmWave rectennas are only able to yield a net DC power of less than 10 mW, the justification for development of mmWave rectennas despite their lower efficiency compared to Ultra-high Frequency (UHF) bands lies in their compactness [6]. Moreover, mmWave transceivers have been reported with as low as 7.2-μW active receiver power consumption [16], in addition to nW-sleep power for Bluetooth Low Energy transceiver [17]. Furthermore, a low data rate 60 GHz transceiver has been reported with a 4.9 pJ/bit energy consumption at 60 GHz [18]. Therefore, developing an unobtrusive wearable mmWave rectenna, with a net DC output across a broad bandwidth using low-cost materials and commercial components is paramount for enabling mmWave RFEH.

In this paper, rectenna development for 5G RFEH and WPT is presented. A broadband textile antenna is presented for wearable applications, the first textile-based antenna covering the 5G spectrum. The rectenna is integrated with a fully-distributed microstrip voltage doubler rectifier based on a commercial Schottky diode demonstrating a 1.3-V DC output from less than 12 dBm of mmWave power across the full bandwidth between 20 and 26.5 GHz, and more than 1-V from under 10 dBm from 23 to 24.5 GHz.

In addition to the contributions in [19], this paper presents substantial extensions in improving original broadband high-efficiency antenna design, for more stable radiation patterns, efficiency and gain, independent of separation from the human body, in sections II and III. Additional analysis of the proposed antenna and comparisons to a standard patch antenna are presented.

The main novel contribution is the design and implementation of a broadband mmWave rectifier using a fully-distributed elements microstrip matching network, for compatibility with a standard 50Ω antenna, presented in section IV. This work demonstrates the first textile-based, flexible mmWave rectenna for wearable RFEH applications in future 5G mmWave bands (section V), and the first rectenna with broadband (28% fractional bandwidth) 1.3 V DC sensitivity from 12 dBm of wireless power above 20 GHz.

II. Antenna Design and Fabrication

A. High-Efficiency, Broadband Antenna Design

5G mmWave bands are motivated by the wider available spectrum. In Europe, China, Africa and Brazil, 26 GHz is chosen as a center frequency while in the US, Japan, South Korea and India the legislated frequency is 28 GHz [20]. In addition, 1 GHz bandwidth will be allocated to individual mobile service providers in the so-called mmWave 5G bands [20]. Collectively, the 26 and 28 GHz bands cover a bandwidth of 5.25 GHz, approximately 20% fractional bandwidth. Such wide bandwidth motivates research into broadband antenna design both for communication and wireless power harvesting applications.

In order to realize a rectenna capable of harvesting energy at 5G bands, along with the 24 GHz license-free band, the antenna needs to have a wide impedance bandwidth. Moreover,
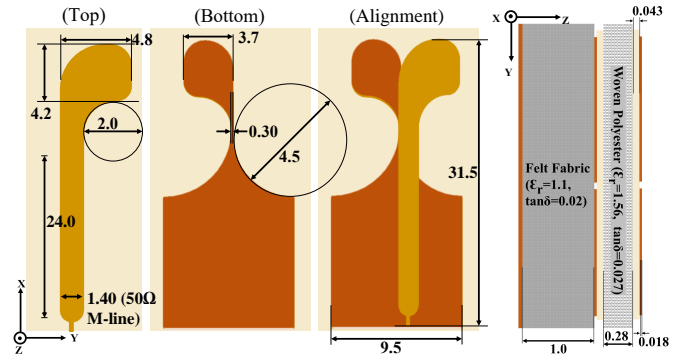

Fig. 1. The proposed antenna layout and dimensions (in mm), showing the double-sided AVA and the substrate composition
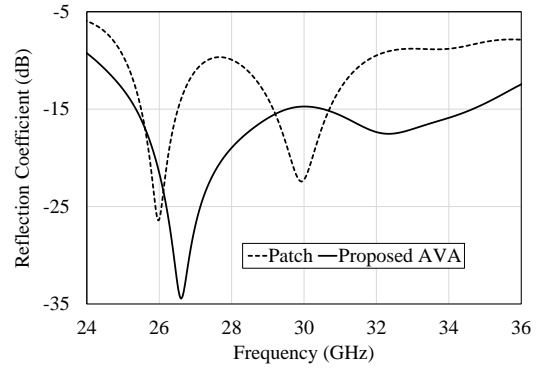

Fig. 2. Simulated reflection coefficient of the two antenna designs considered, a common-geometry patch and the proposed novel AVA.

as a textile or flexible rectenna may be used in proximity with human tissue, a frequency-independent antenna is preferred to minimize any detuning impact. The proposed antenna is based on the broadband Antipodal Vivaldi Antenna (AVA) [21]. Although the antenna's geometry is not self-complimentary or symmetric due the 50Ω microstrip line width being comparable to the radiator, resulting in a narrower bandwidth, the radiator's shape and size have been tuned in 3D full-wave simulation to achieve a bandwidth covering the 24, 28 and 36 GHz bands.

The main aim of the antenna design process has been to prioritize maximizing the radiation efficiency. Given the high tanδ of textile substrates [22], this has been achieved by choosing an antenna design where a minimum part of the radiator is parallel to the ground-plane (e.g. a monopole) to minimize the electric field dissipation in the substrate. This is explored in comparison to a standard patch antenna in Section II-B. The AVA's layout and dimensions are shown in Fig. 1.

B. Comparison with a Standard Patch Antenna

For benchmarking purpose, a standard microstrip patch antenna has been simulated to validate the assumptions on the influence of the radiator's area on the antenna's efficiency, and to demonstrate the improvement of the proposed design over a standard design on the same substrate. Patch antennas have been widely reported in wearable mmWave antennas [23] and in low-cost additively manufactured rectennas [12], [14],
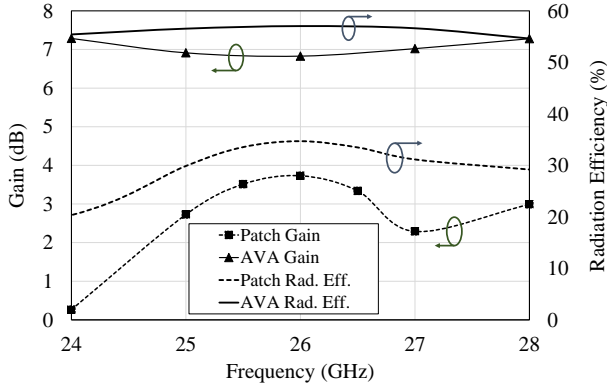
Fig. 3. Simulated gain and radiation efficiency of the patch antenna and the proposed AVA at the frequencies of interest.

[15]. The patch's dimensions are 9×7.125 mm with a 3.25 mm inset microstrip feed. Both antennas have been simulated using CST Microwave Studio using the measured substrate properties ($\epsilon_r = 1.67$ and $\tan\delta = 0.027$). Fig. 2 shows the simulated reflection coefficient of the antennas. The gain and radiation efficiency are shown in Fig. 3.

Overall, a more broadband behavior is expected from the proposed AVA, as demonstrated by the lower reflection co-efficient in Fig. 2 and more stable gain in Fig. 3. However, at 26 GHz, where both antennas achieve $S_{11} < -20$ dB, the proposed AVA achieves over 67% higher radiation efficiency relative to the patch antenna. This in-turn affects the antenna's gain demonstrating more than 3 dB gain improvement by the proposed antenna design over a common geometry patch. This is explained by the patch antenna's higher dielectric losses discussed earlier; over 53.7% of the accepted power is dissipated in the patch's textile substrate as opposed to only 32.4% of the power accepted by the proposed AVA.

C. On-Body Antenna Isolation

Obtaining stable off-body broadside radiation patterns is essential for efficient wearable rectenna operation. In [19], a novel approach of employing the human body as a reflector has been devised to improve the antenna's efficiency, bandwidth, and gain at the frequencies of interest. This has been achieved using asymmetric alignment of the radiator arms to allow the far-fields to reflect off the human body, hence improving the gain. However, this approach is only valid when the antenna is separated from the human body by more than 4 mm, which cannot be guaranteed in all modes of operation.

In order to ensure the antenna maintains stable radiation patterns and bandwidth in the presence and absence of the human body, an additional metal reflector layer is proposed. Thus, broadside radiation patterns can be achieved by the monopole at its fundamental frequency. Metalized microwave shielding fabric (copper and nickel coated) has been used for the reflector plane. Shielding fabrics are chosen as they are breathable, more user-friendly compared to copper sheets and, in this case, do not need to be patterned to produce small features.
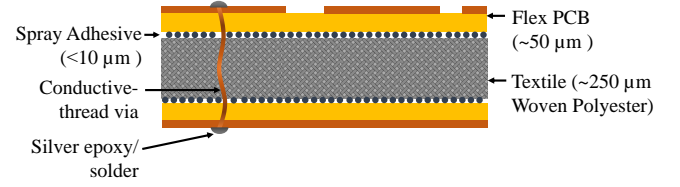

Fig. 4. Cross-section of the antenna showing the multi-layer substrate and the through-textile via.
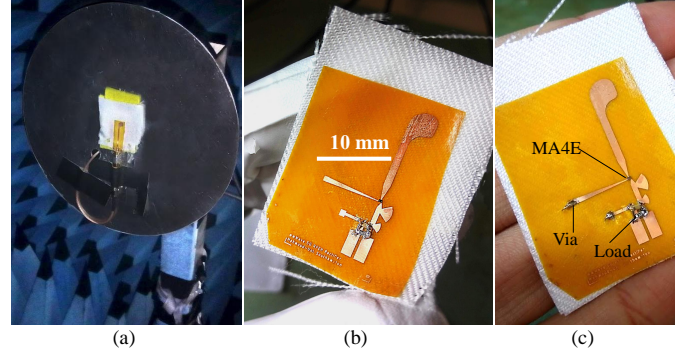

Fig. 5. Photographs of: (a) the connectorized antenna used for S_{11} and radiation properties measurements, (b) the rectenna after mounting components before adding the through-textile via, (c) the rectenna used in the wireless testing.

The minimum separation between the antenna and the reflector has been set to 1 mm ($0.08 \times \lambda_0$/ at 24 GHz). A 1 mm felt fabric (of lower $\tan\delta$ compared to woven polyester) has been inserted between the antenna and the reflector as shown in Fig. 1 to support the reflector. While the additional fabric layer will degrade the antenna's radiation efficiency (due to the additional dielectric losses), the effect is expected to be minimal compared to degradation in the efficiency due to absorption by the human body.

D. Antenna Fabrication

Among the candidates for the antenna's fabrication methods are screen and inkjet-printing [24], woven or adhered conductive textiles and copper foils [22], [23], as well as etched Kapton copper laminates [25]–[27]. To produce smooth and homogeneous conductors, a high resolution process is crucial at mmWave bands, where the feature size is commonly less than 1 mm. Therefore, manufacturing tolerances, surface roughness and non-uniformities need to be minimized as they can significantly affect the antenna's performance. As textile substrates are porous and have high surface roughness, conductor printing has been excluded due to the high thickness of the required interface layer, resulting in higher dielectric losses and reduced antenna efficiency [22].

Ultra-thin polyimide copper laminates exhibit improved flexibility compared to copper foils, and lower thickness compared to printed interface layers, minimizing dielectric losses. The antenna is fabricated on the polyimide laminates using a standard photolithography process, with the track's pattern plotted on a dark-film mask. A minimum feature size of 150 μm is achieved using standard PCB manufacturing

equipment. After the adhesion of the flexible circuit onto the textile substrate, the via holes are drilled and conductive thread is inserted to form the conductor. The antenna has been fabricated using the standard photolithography process described in [19], [26]. However, to realize the double-sided voltage doubler rectifier, conductive threads are utilized to create DC vias, solder paste has been used to connect the via (thread) to the copper traces on the top and bottom layers. Fig. 4 shows a cross-section of the structure. The fabricated antenna and rectenna prototypes are shown in Fig. 5.

While the fabrication processes reported in [23] and [28] can produce antenna's with re-producable 0.2 mm-sized features, they utilize copper foils and embroidered conductive threads, respectively. The proposed method utilizing polyimide-copper laminates allows over-all thinner and lighter conductors compared to the 80 μm foil in [29], and the 120 μm thread in [28]. In addition, the low surface roughness of copper laminates (<1 μm) and higher conductivity than conductive textiles imply lower conductor losses and therefore improved antenna efficiency. Furthermore, the reliability of electronic systems realized using polyimide laminates and encapsulated using glob-top has been extensively studied in [30] showing sustained functionality over more than 1000 bending cycles.

Although the textile substrate in use has previously been characterized at 2.45 GHz in [22], the inhomogeneity of textiles mean that a new two-line characterization [31] of the sample needed to be performed. Two microstrip lines, of approximately 50Ω impedance were built and measured. the extracted dielectric properties exclude the impedance mismatch losses due to additional reflection at the coax-microstrip interface. The measured insertion loss is 0.90 dB/cm and 1.79 dB/cm at 28 GHz and 60 GHz respectively, only 0.11 dB/cm higher at 60 GHz than reported in [23]. The dielectric properties of the polyimide-woven polyester sandwich substrate utilized is $\epsilon_r = 1.67$ and $\tan\delta = 0.027$.

III. Antenna Simulation and Measurement

The 3D model of the antenna has been simulated using full-wave electromagnetic simulation in CST Microwave Studio. The 1.85 mm connector used to measure the fabricated antenna has been included in the antenna's model to observe its effect both on the antenna's impedance bandwidth and on the radiation patterns, in addition to obtaining a closer match with the measured results for validating the simulation model. A human skin layer, based on CST's Voxel library has been added to investigate the effect of human proximity on the antenna. As a significant portion mmWaves do not penetrate deeper than skin layers due to absorption [32], only the skin layer has been included in the model. Furthermore, as the antenna utilizes a solid reflector plane, minimal power from the antenna's power would be absorbed by the body. When the antenna is simulated at 4 mm from the skin in CST Microwave Studio [19], 1% of the accepted power by the antenna has been absorbed by the skin layer.

The fabricated antenna has been measured using a E8361A 67 GHz PNA Vector Network Analyser (VNA), calibrated using a standard Short, Open, Load, Through (SOLT) electronic
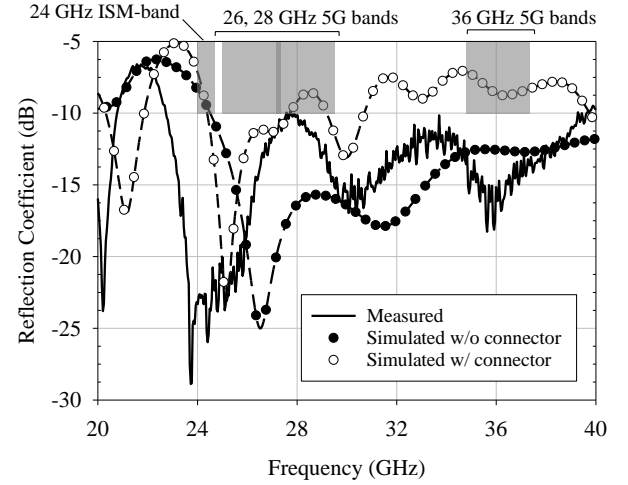
Fig. 6. Simulated (dashed) with (w/) and without (w/o) the connector, and measured (solid) reflection coefficient of the proposed textile mmWave antenna.

calibration kit. The 1.85 mm connector has been soldered to the bottom ground plane using a uniform solder layer to avoid impedance mismatch at the coax-microstrip transition. Fig. 6 shows the simulated and measured reflection coefficient of the antenna, showing a S_{11} bandwidth covering the full 5G spectrum up to 40 GHz. The deviation in the measured results could be attributed to the connector being of comparable size to the antenna's radiator, and the additional reflection due to standing waves in the test-cable (resulting in the ripples around 24 and 32 GHz). Nevertheless, the simulation and measurements agree in covering the required S_{11} bandwidth of 24 GHz and 5G RFEH. Furthermore, the level of agreement at the frequency bands of interest is consistent with similar designs such as the 24 GHz antenna array in [7]. The S_{11} measurements have been performed with the antenna placed on a human hand and no change has been observed on the measured S_{11}, this has also been previously presented in [19] despite the reduced isolation over the proposed reflector-backed AVA.

For evaluating the far-field properties of the AVA, two designs have been considered: the 25-mm microstrip-fed AVA in Fig. 1 (simulated and measured), and the same antenna with a short 5-mm feed to match the antenna integrated in the final rectenna (simulated). The longer feed sample has been used for model-validation through 3D far-field measurements, to avoid distortion to the measurements due to the connector size.

The 3D polarimetric far-field radiation patterns of the antenna have been measured in an anechoic chamber, at 24 GHz, and simulated using CST's field monitors. A WR-42 horn antenna has been used as a reference for the anechoic chamber measurements (Fig. 5). An extended microstrip feed-line of 25 mm has been included to mitigate distortion from the connector to the radiation patterns [23]. However, the insertion losses in the microstrip line are expected to reduce the measured radiation efficiency of the antenna. The efficiency of the proposed textile antenna has been measured with respect to the horn antenna to be 67%, including the -1.5 dB losses

24 GHz

26 GHz
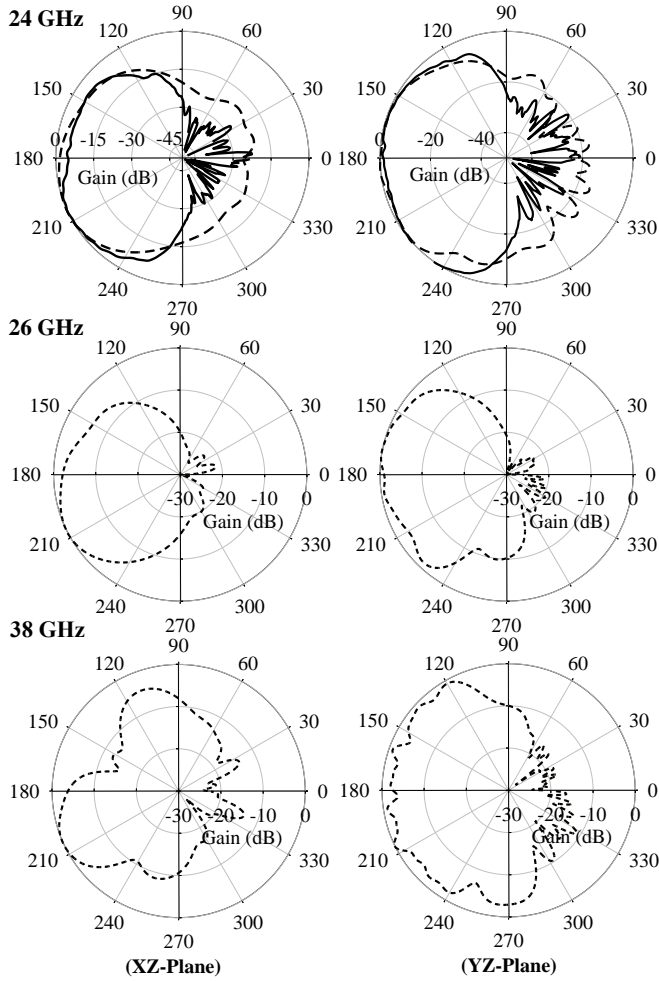
38 GHz

(XZ-Plane) (YZ-Plane)

Fig. 7. Normalized simulated (dashed) and measured (solid) gain of the proposed AVA at: (a) 24, (b) 26 and (c) 36 GHz, on the XZ and YZ planes of the antenna.
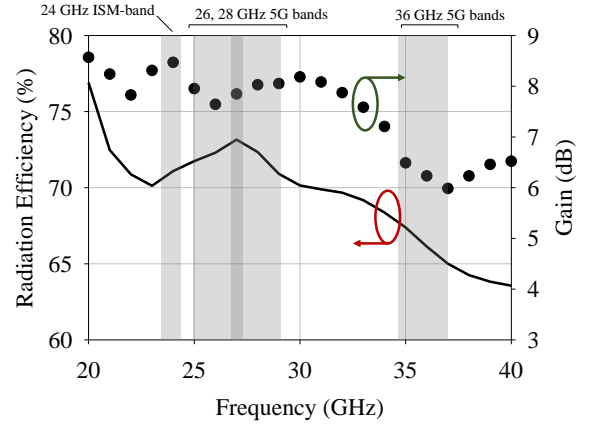

Fig. 8. De-embedded radiation efficiency and gain of the proposed AVA, on-body, with a 5 mm microstrip feed matching the rectifier's feed length.

TABLE I
COMPARISON OF THE PROPOSED ANTENNA MEASURED PROPERTIES WITH STATE-OF-THE-ART PRINTED AND TEXTILE ANTENNAS

	This work	2019 [33]	2013 [23]	2012 [34]
BW (GHz)	23-40 (54.0%)	26-40 (42.4%)	55-65 (16.7%)	57-64 (11.6%)
Antenna	AVA	CPW monopole	2×2 patch	Yagi-Uda
Substrate	Textile ($\tan\delta$=0.027)	LCP ($\tan\delta$=0.002)	Textile ($\tan\delta$=0.02)	Textile ($\tan\delta$=0.016)
Gain (dB)	7.41*, 8.47†	8.76	7.8	11.9
Radiation pattern	Broadside single-beam	Broadside two-beams	Broadside single-beam	End-fire
Efficiency	67%*, 73%†	90% (simulated)	41%	48%
Electric dimensions (λ_0)	$3.0\lambda_0 \times 0.94\lambda_0$	$1.12\lambda_0 \times 1.02\lambda_0$‡	$4.26\lambda_0 \times 1.03\lambda_0$	$5.2\lambda_0 \times 1.6\lambda_0$

*Measured: antenna+25 mm microstrip, †Simulated antenna+5 mm microstrip
‡Small length due to the miniaturized CPW feed and connector's ground.

in the prolonged microstrip feed. The normalized gain patterns of the antenna at 24, 28 and 36 GHz are shown in Fig. 7. Both the simulated and measured radiation patterns show over 20 dB front-to-back ratio, implying minimal interaction between the antenna's broadside radiation and the human body shielded by the reflector. The computed radiation efficiency and gain (validated by the de-embedded measured radiation patterns and efficiency agreement with the simulated results) are shown in Fig. 8. The only discrepancy observed between the simulated and measured radiation properties is the higher back-radiation in the simulated model, due to the smaller size of the reflector in the model to reduce the problem's mesh size. However, in real-life operation and in the measured prototype, the textile reflector could be electrically large minimizing the back-lobe radiation as observed in the measured plots.

From the rectenna's radiation properties shown in Fig. 8 (excluding the simulated insertion losses in the long feed-line), the antenna achieves a radiation efficiency of more than 70% up to 30 GHz, peaking at 73.4% at 26 GHz. The decay in efficiency at higher frequencies is due to the increase in the dielectric losses in the substrate. The proposed antenna with the reflector plane achieves slightly lower efficiency

than the previously simulated 77% in [19]. However, the solid reflector results in more stable radiation properties over the full bandwidth, as observed in Fig. 8, in addition to guaranteeing that the achieved efficiency does not degrade in human proximity.

Table I compares the performance of the proposed AVA against reported textile-based and additively manufactured low-cost mmWave antennas. It can be seen that the proposed antenna achieves the highest radiation efficiency compared to the reported antennas implemented on low-cost substrates. The antenna in [33] is able to achieve efficiencies higher than 90% due to the low loss substrate and its CPW geometry. To add, the smaller length of [33] does not include a sufficiently large ground plane due to the coax connector acting as a ground plane for the antenna in simulation and measurement.

IV. TEXTILE MMWAVE RECTIFIER

A. Diode Selection and Modeling

The main criteria when choosing a diode at mmWave bands is the high cut-off frequency of the diode, otherwise the diode will not act as a rectifying element and the high-frequency

signal will be able to propagate to the output through the diode and package parasitics. While the cut-off frequency is the frequency when the real and imaginary components of the diode impedance are equal, the diode's Power Conversion Efficiency (PCE) will be adversely reduced at frequencies approaching $f_{cut-off}$. Moreover, a significant portion of the energy at the output will always exist at the 1st and 2nd harmonics and not at DC [8], implying that proper harmonic termination is implemented at the output [7], [12], [14]. The cut-off frequency is defined in this work as the frequency where the resistance and the reactance of the diode are equal, and is given by

$$f_{cut-off} = \frac{1}{2\pi R_S C_T}, \quad (1)$$

where C_T is the diode's total capacitance and R_S is the series resistance [35], [36]. While in [36] only the junction capacitance is considered due to the devices being measured on-wafer, when the diodes are packaged the total (junction+packaging) capacitance needs to be considered.

Two diodes have been considered for the rectifying element: a Silicon Skyworks SMS7630 and a Gallium Arsenide (GaAs) Macom MA4E-1319, recommended by the manufacturers for detector applications above 26 and 80 GHz, respectively. Extensive analytical and experimental analysis of the PCE of different rectifiers (including the SMS7630 and MA4E) is presented in [37]. The purpose of the input impedance simulation is to highlight the variation in the performance of the diodes when the packaging parasitics are considered, which is particularly important in a flexible textile-based system. The MA4E has previously been simulated demonstrating the highest PCE compared to commercial Si diodes at 24 GHz [38]. The diodes have been simulated, in a single series topology, in ADS using Harmonic Balance simulation. Both 50Ω source and load impedance were used to match the measurement setup of the two-port s-parameters.

To maximize the simulation accuracy between 20 and 30 GHz, the diode models were based on the datasheet SPICE parameters, and optimized models using the available measured s-parameters (SMS7630) and the IV-curves (MA4E) [12]. Fig. 9 shows the simulated input impedance of the SMS7630 and the MA4E, based on the 0 dBm s-parameters and the IV-curve, respectively, when terminated with an ideal 50Ω load. The Smith chart in Fig. 9 shows the cut-off region of the diodes' impedance (striped shading) and the rectification region (solid-green shading). The diode parameters used in the non-linear simulations in this work are C_j=0.02 pF R_S=9Ω for the junction capacitance and series resistance, and C_P=0.035 pF L_P=0.3 nH for the packaging capacitance and inductance.

It can be observed that although the SMS7630 junction (datasheet parameters) is capable of rectification up to 24 GHz (impedance falling in the solid-green shaded region in Fig. 9). However, when the packaged diode's parasitics are taken into consideration, the diode acts as a short-circuit allowing the 1st order harmonics to propagate to the output. The MA4E1319 on the other hand is usable up to 40 GHz (based on the Large-Signal S-Parameters LSSP-simulation using the parameters from [12]), yet the packaging parasitics show significant
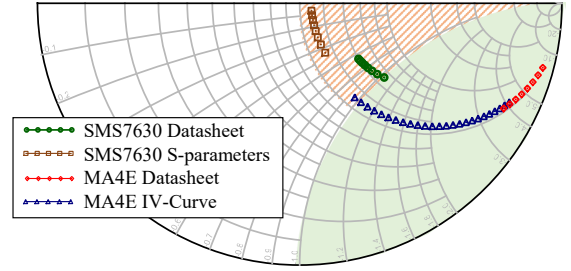

Fig. 9. Simulated (LSSP) input impedance of the SMS7630 and MA4E diodes from 20 to 40 GHz, using diode parameters from the datasheet as well as the optimized models based on experimental characterization.
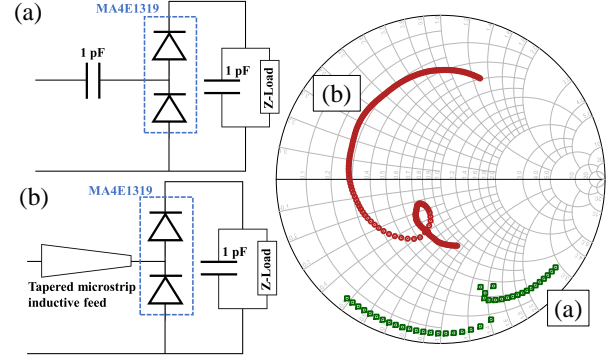

Fig. 10. Schematic of the voltage doubler and Smith charts showing the impedance matching approach, for a 10 kΩ load, of: (a) conventional voltage doubler, (b) rectifier with the tapered matching line and distributed microstrip input capacitance.

discrepancy with the datasheet model of the junction which can be used through 100 GHz. The discrepancies could be attributed to the diode's mounting imperfections while the manufacturer's parameters are measured on-wafer.

B. Rectifier Design

The MA4E-1319 has been chosen as the rectifying element in this work. With two diode's integrated in the same die, it is expected that the external parasitics will be lower improving the cut-off frequency of the diode. The voltage doubler's impedance, seen on the Smith chart in Fig. 10-a, is predominantly capacitive. Therefore, a high-impedance inductive matching network is required. Moreover, the 1 pF input capacitance can be achieved using the microstrip feed's own distributed capacitance. A tapered microstrip line could be used to match the impedance of the rectifier as in Fig. 10-b, stepping-up the impedance of the rectifier to match the 50Ω source, as well as conjugating the capacitive diode impedance using the microstrip line's own inductance.

A key challenge in broadband impedance matching is the trade-off between bandwidth and Quality factor, where a sufficiently low S_{11} may not be achievable over a wide range of frequencies. The theoretical limit on the minimum achievable reflection coefficient of a load is given by the Bode-Fano return-loss limit,

$$|\Gamma_m| \geq e^{\frac{-1}{2BRC}} \quad (2)$$

$$S_{11} \geq 20\log(\Gamma_m), \quad (3)$$

a function of the bandwidth *B*, and the equivalent RC circuit of the load. The load in this case is the voltage doubler and the DC load.

Harmonic balance simulation was used to extract the rectifier's impedance (Fig. 10-a), the bandwidth *B* has been set to 4 GHz (24-28 GHz). The equivalent RC circuit of the rectifier in Fig. 10-a has been extracted using optimization of an RC load with tunable resistance and capacitance, to match the simulated LSSP; the extracted values are R=904Ω and C=0.161 pF. The calculated minimum achievable Fano S_{11} is -7.5 dB ($\Gamma_m \geq 0.42$). While in [39] the increase in the number of diodes has been studied in order to increase the return loss of a rectifier through reducing *R*, this approach is not possible at mmWave frequencies due to the higher losses incurred in the additional rectifier stages. In [40], the impact of the diode's model on the maximum achievable bandwidth and return loss is studied, showing that a diode with lower parasitics, such as the VDI ZBD, can achieve over 10$\times$ higher bandwidth compared to the SMS7630. However, the high cost of the W-band VDI ZBD diode makes it impractical for low-cost wearable IoT applications. Therefore the MA4E is selected.

In order to step up the input impedance of the 50Ω source and achieve an inductive feed-line, the microstrip line feeding the diode is tapered to gradually increase the inductance of the source. A tapered line is also used at the ground connection of the voltage doubler, the length of the tapered lines has been optimized in simulation to achieve an impedance match between the 50Ω antenna and the rectifier at the frequencies of interest. While an L-matching network could be used to achieve a high Q-factor matching, improving the PCE at low P_{RF} levels as in [7] and [41], a wide bandwidth rectifier is prioritized in order to demonstrate the feasibility of harvesting from a broad bandwidth to meet 5G RFEH requirements.

In order to prevent the high-frequency component of the input from propagating to the output, significantly reducing the net DC output, radial stubs ($\lambda/4$ at 26 and 52 GHz) are utilized for harmonic rejection at the output. The DC test pads included at the output, to allow measuring the voltage across the load, were found to not have any effect on the rectifier's performance in simulation. Fig. 11 shows the layout of the rectifier, and the modified antenna ground plane to accommodate the rectifier. As the ground via is for the DC return current, the impedance matching of the vias is not critical. Furthermore, different thicknesses, resistances, and inductances of the vias have been studied in ADS and were found to have minimal impact on the rectifier's performance.

In terms of textile coverage and breathability, the proposed rectenna occupies a small area of 16 x 33 mm^2. Thus, should the rectenna be used in a large-area array configuration, a $\lambda_0/2$ (6.25 mm at 24 GHz) would imply a coverage of less than 60% of the total area of the garment. Furthermore, [30] has shown scalable integration of polyimide-circuit filaments in standard textile weaves for improved integration, user-comfort and reliability.

C. Rectifier Simulation and Measurement

The return loss of the 1.85-mm connector-fed textile rectifier prototype has been measured using a VNA. Due to additional
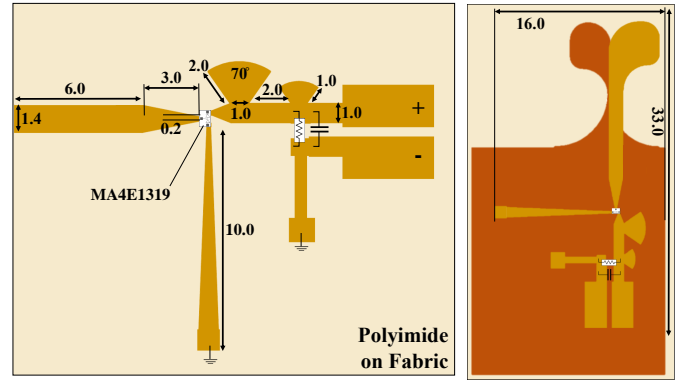

Fig. 11. The dimensions, in mm, of the proposed textile-based 5G rectifier (left) and the integrated rectenna layout (right).
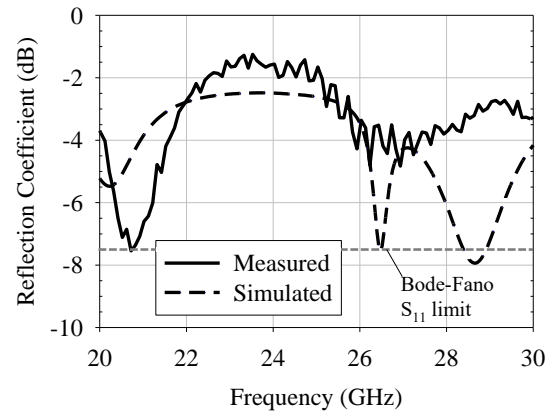

Fig. 12. Measured and simulated reflection coefficient of the rectifier at -5 dBm.

incurred cable losses at 28 GHz and the VNA's power limit, the maximum power deliverable by the VNA is -5 dBm. Fig. 12 shows the simulated and measured S_{11} of the rectifier. The connector has been modeled as a tapered microstrip line of 5 mm length. While the observed reflection is higher than 3 dB, this is attributed to the wide variation in the input impedance of the rectifier due to its large electric length, impeding a sufficiently low S_{11}, in addition to the Bode-Fano theoretical limit on the minimum reflection calculated to be above -7.45 dB.

In order to measure the PCE of the rectifier, the DC voltage across the load has been measured using an oscilloscope. A Wiltron 68069B Continuous Wave (CW) signal generator (providing up to 13 dBm) has been used to provide sufficient power to investigate the performance of the connectorized rectifier. A Keysight N8485A 33 GHz power meter has been used for power-calibration and for measuring the net power available at the rectifier's input after factoring in cabling and unleveled output losses, reducing the uncertainty in the mmWave power level to ±0.1 dB. Due to the low thickness of the substrate compared to a standard 1.6 mm board connector, the coax interface introduces additional 0.1 nH inductance (modeled in CST) reducing the rectifier's impedance matching. The power has been swept from 0 dBm to the setup's maximum output of 13 dBm. Fig. 13 shows the measured DC output, across a
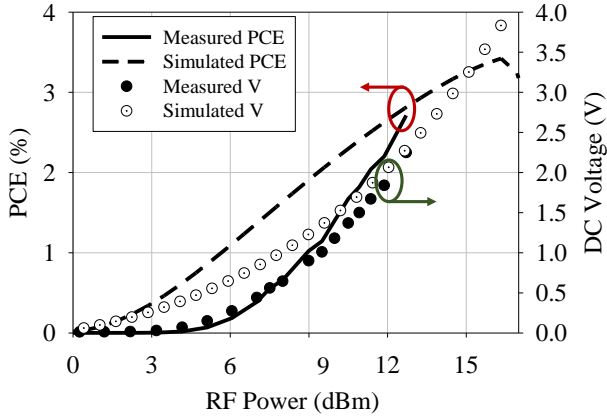
Fig. 13. Measured and simulated PCE of the rectifier and the DC voltage across a 10 kΩ load at 24 GHz with a coax connector.
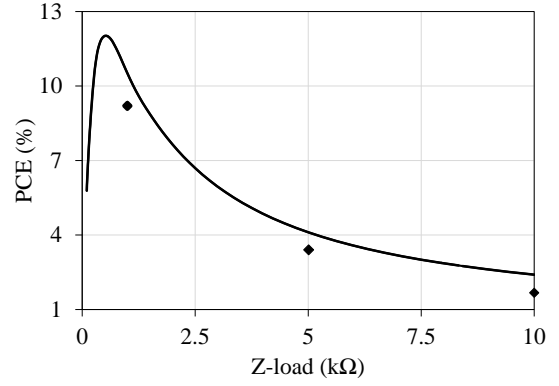

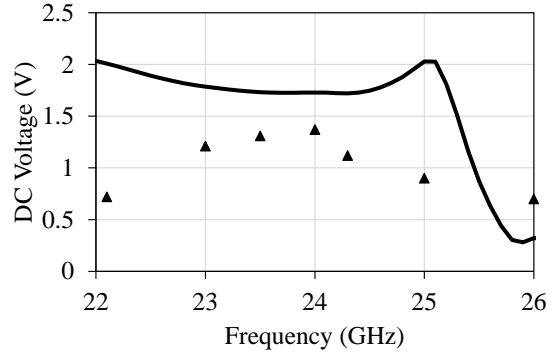Fig. 14. Simulated (solid line) and measured (discrete points) PCE for variable load impedance at 10 dBm.

Fig. 15. Simulated (solid line) and measured (discrete points) DC voltage output of the connector-fed textile rectifier at 10 dBm with a 10 kΩ load.

10 kΩ resistor, at 24 GHz.

Above 10 dBm of input power, it can been seen that the simulated output voltage matches, within 10%, the measured values. The agreement between simulation and measurement shown in Fig. 13 at 10 dBm is higher than that in [7] and [42], where approximately 25% discrepancy has been reported in the measured voltage output compared to simulation, despite them being implemented on rigid low-loss substrates. This validates the proposed rectifier's performance and design approach for flexible lossy textile substrates. The discrepancy between the simulation and measurement at lower power levels can be attributed to:

1) Inaccuracy in modeling the connector in the Harmonic Balance simulation altering the rectifier's input impedance resulting in additional reflection.
2) Inaccuracy of the MA4E junction and packaging resistance and capacitance at low mmWave power levels reducing the PCE.
3) The imperfect connection between the diodes' pads and the microstrip lines resulting in additional series resistance.

When considering the theoretical limit on the received power, the PCE can be calculated using (4). The DC power is referenced to the theoretical maximum accepted power after factoring out Fano's reflection limit using

$$PCE_{Fano} = \frac{P_{DC}}{(1 - |\Gamma_m|^2)P_{RF}}, \tag{4}$$

instead of the power available from the generator.

The maximum PCE_{Fano} achieved by the rectifier at 24 GHz is 14% at 12.7 dBm, with a net DC output of 0.5 mW, sufficient for low-power nodes and transceivers in [16]–[18].

The output of the rectifier has been investigated at different load impedances. Fig. 14 shows the PCE of the rectifier at 24 GHz for different load impedances at 10 dBm. The higher optimal load impedance of the proposed rectifier compared to the reported mmWave rectifiers (Table II), due to the voltage doubler, configuration results in the improved 1-V sensitivity.

In order to evaluate the rectifier's capability of harvesting energy across a broad bandwidth for 5G applications, the frequency of the CW single-tone input to the rectifier has been varied. The load impedance of the broadband rectifier has been set to 10 kΩ, despite the reduced PCE, for improved voltage sensitivity. Fig. 15 shows the output voltage of the rectifier from 22 to 26 GHz.

While the measured output voltage at 24 GHz approaches the simulated value, the rectifier's DC output is cut-off at frequencies higher than 24.5 GHz even though its input impedance matching is expected to be maintained based on the small-signal S_{11} in Fig. 12. This is attributed to the coax-microstrip connector interface resulting in lower output voltage at frequencies above 24 GHz. Therefore, the broadband wireless testing in the next section has been performed to overcome the additional measurement uncertainties introduced by the coax connector.

V. RECTENNA WIRELESS TESTING AND EVALUATION

A. Rectenna Experimental Testing

The integrated rectenna has been tested using the CW generator, connected to a Keysight 83020A Power Amplifiers (PA), capable of producing up to 27 dBm at 24.5 GHz, and a standard 20 dBi horn antenna. To avoid the PA's gain compression, an additional attenuator was introduced between the CW and the PA to minimize the unleveling of the output and suppress the gain compression effect. Finally, due to the non-linear behavior of the PA and the CW generator at higher power levels, a calibrated RF power meter has been connected
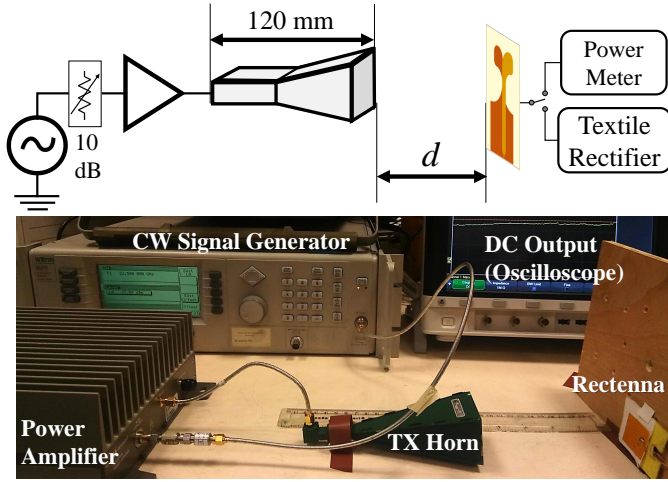
Fig. 16. The wireless test setup schematic and photograph of the textile rectenna.

Fig. 17. Measured DC output of the rectenna at variable separation from the horn antenna.

to the connectorized textile antenna to estimate the power levels at the receiver. The power sensor is rated to a <1.26 standing wave ratio (SWR) up to 26.5 GHz, normalized to 50Ω. Therefore, the textile AVA is matched to the power sensor ensuring accurate incident power level measurements. The mmWave power levels reported in this section are based on the power calibration using the textile AVA connected to the power meter. Fig. 16 shows the rectenna test setup. The 10 cm maximum separation between the horn's radiating aperture and the rectenna, shown in Fig. 16, represents $8 \times \lambda$ at 24 GHz. This is consistent with the separation reported in the wireless testing of the 17 GHz rectenna in [42] with 8.8 λ separation between the horn transmitting antenna and the rectenna.

The distance d has been varied to vary the power level at the rectenna. The distance between the horn's radiating aperture and the coax-waveguide transition is 120 mm. Therefore, the total separation between the rectenna and the CW signal from the PA is d+120 mm. While the power is typically proportional to $1/d^2$, due to the measurements being carried with d being comparable to the horn's dimensions, the far-field gain and path loss models are not accurate. The input power to the PA in this setup has been kept below −17 dBm (−5 dBm signal generator input, −10 dB attenuator and −2 dB cable losses). The power level is below the PA's saturation region to minimize its non-linearity and enhance repeatability. Fig. 17 shows the measured DC output of the rectenna at varying separation, as well as the measured incident mmWave power, at 24 GHz, using the power meter. The distance sweep shows improved voltage-sensitivity over the mmWave rectenna in [41], tested using a 42 dBm Equivalent Isotropically Radiated Power (EIRP) with a 25 dB horn, by more than 1-V at 20-mm separation from the horn's radiating aperture. CW excitations have been previously utilized to test the performance of broadband rectifiers in [39], [42].

To evaluate the rectenna's performance at higher power levels, the CW signal generator output has been increased until a 20 dBm is observed on the wireless power meter. At 24 GHz, from an incident power of 20 dBm, the rectenna achieves more
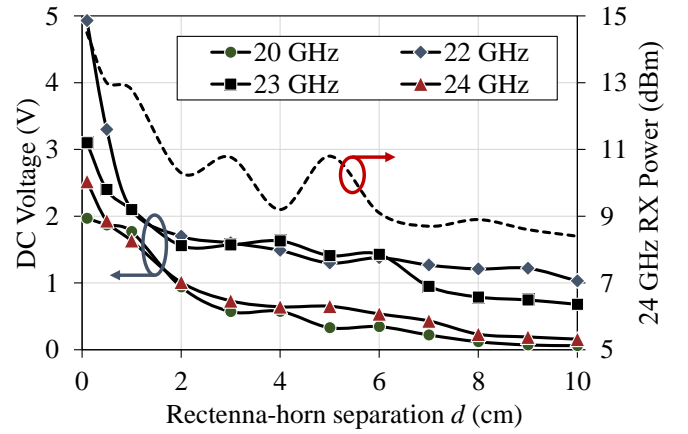
than 6.5V with a 10 kΩ load. This is the highest reported output voltage of a low-power rectenna operating between 20 and 30 GHz. The measured DC output of the 10 kΩ-loaded rectenna is 6.5, 5.7, 4.6 and 4.2 volts from 20, 19, 18, and 16 dBm, respectively. These results have been measured using the test setup in Fig. 16 with the power levels based on the measurement using the power meter.

In order to demonstrate the rectenna's capability of broadband harvesting across the full mmWave 5G spectrum. A broadband frequency sweep has been performed using the wireless setup in Fig. 16. The rectenna has been placed at d=1 cm from the horn antenna. To estimate the mmWave power level at the input, the calibrated power meter has been connected to the 50Ω textile AVA and positioned in the same place as the rectenna.

As the AVA is in the horn's radiative near-field region, the test setup (horn+AVA) has been simulated in CST Microwave Studio to quantify the S_{21} for additional validation. At 24.5 GHz, the simulated $S_{21} + PA'$soutput shows a ±1 dB agreement with the 12 dBm measured input power using the power sensor. Details of the test setup model are included in the supplementary material. The power from the CW has been configured at individual measurement points, to overcome the variation in the path loss and the antennas' coupling, to ensure approximately 12 dBm of power is available at the rectenna. Through this power calibration, the gain-compression and PA's non-linearities could be overcome.

As the measured power by the detector is absorbed by its 50Ω port termination, a different power level will be accepted by the textile rectifier. However, as the textile AVA is matched to a 50Ω characteristic impedance across its usable bandwidth to simplify measurements, the rectifier's input power (the AVA's microstrip feed) will match that measured by the power sensor. Any variations in the power accepted by the diode will be a function of the impedance matching of the rectifier. While the power evaluation could be performed using a standard gain reference horn antenna, the non-planar geometry of the horn antenna complicates the calculation of the path losses and subsequently the positioning of the rectenna when performing the DC measurements. To explain, as the distance between

TABLE II
COMPARISON OF THE PROPOSED TEXTILE RECTENNA WITH STATE-OF-THE-ART mmWAVE ENERGY HARVESTERS ABOVE 20 GHz.

|	This Work	TCAS 2014 [7]	AWPL 2014 [41]	WPTC 2017 [12]	IMS 2019 [14]
Antenna Design	Broadband AVA (single element)	Cavity-backed 2×2 patch array	4×4 patch array	2×2 patch array	2×1 patch array
Substrate	Textile (ϵ_r = 1.67, $\tan\delta$ = 0.027)	Rogers Duroid (tanδ=0.001)	Rogers Duroid (tanδ=0.001)	LCP (tanδ=0.003)	3D printed FLGR02 (ϵ_r=2.83, tanδ=0.03)
Diode	MA4E-1319	MA4E-1317	MA4E-1317	MA4E-2038	MA4E-2038
Frequency Bands (GHz)	Antenna: 22.6-40, rectifier: 20-26.5	24	35	24	28
1-V Sensitivity	9.5 dBm (24 GHz)	11.9 dBm	2.8 mW	11 dBm	12.5 dBm
Maximum DC Voltage	6.5V (20 dBm)	1.2V (13 dBm)	2.2 V (8.45 dBm)	2.58V (18 dBm)	2.1V (17 dBm)
Load (kΩ)	10, 0.63	0.16	1	0.739	750
10 dBm PCE	12% (24 GHz, 630Ω)	24%	67% (7 mW)	7.6%*	<0.1%*
Rectenna 1-V Bandwidth	6.5 GHz (20-26.5 GHz)	Single-tone	1 GHz	Single-tone	Single-tone
Rectenna Half Power Bandwidth	3.5 GHz (15% fractional bandwidth)	Single-tone	Not reported	Single-tone	Single-tone
Electrical Size (relative to free-space λ)	2.6λ×1.3λ	4.4λ×4λ	2.56λ×4.9	2.96λ×0.89λ	Not reported
Area (L×W, mm^2)	32.6×16	55×50	22×42	37×11.1	Not reported

*Calculated from the DC voltage curve
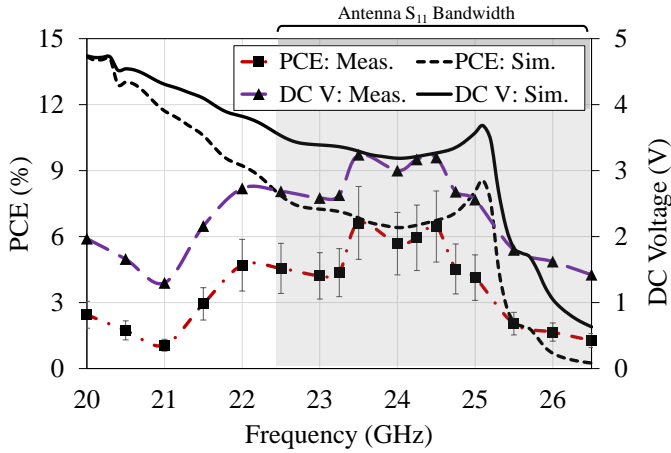
Fig. 18. Measured PCE and DC voltage output of the rectenna from 12 dBm of wireless power, showing more than 1 V output from 20 to 26.5 GHz.

the coax-waveguide transition feeding the horn and the horn's aperture is 120 mm (larger than d in Fig. 16), identifying a rectenna position where the measured gain of the AVA can be used instead of the horn's would be difficult.

Fig. 18 shows the broadband measured DC voltage the PCE. The error bars reflect the ±1 dB uncertainty in the incident power level, matching the 1 dB discrepancy between the path loss simulations and measurements. This demonstrates the rectenna's ability to produce over 1.3 V DC across the 10kΩ load resistor, from 12 dBm of power with PCE varying between 1 and 6.3% validating its broadband performance. From the measured PCE in Fig. 18, the rectenna achieves a 15% half-power (−3 dB) bandwidth from 21.5 to 25 GHz.

The simulated values in Fig. 18 were obtained from the ADS model of the rectifier excluding the antenna. However, as the textile AVA is 50Ω and the wireless power has been measured using the power meter, the results are expected to agree within the ±1 dB wireless power uncertainty. The main discrepancy between the simulation and measurements shows

up below 23 GHz. This is attributed to the proposed antenna, which was only designed and characterized for operation from 24 GHz. Thus, the PCE in this case is bottle-necked by the antenna. The rectifier design can be integrated with a different antenna should it be used below 24 GHz. Above 25.5 GHz, the measured output is observed to exceed the simulated output of the rectifier. This could be attributed to the shorter feed-length of the rectifier, when considering the antenna's 50Ω feed, and the inaccuracies from the resistive and capacitive load mounting. Previously reported mmWave rectennas at 24 GHz [12], and 94 GHz rectenna [43], have shown a measured DC output higher than the simulated due to overestimating the diode's parasitics.

The measurements were limited to 26.5 GHz due to the PA's and the waveguide horn antenna's maximum frequency. However, as the rectenna achieves more than 1.4 V at 26.5 GHz, it is predicted that the rectenna's cut-off frequency is beyond 27 GHz, demonstrating its capability of harvesting across the full 5G spectrum. Moreover, the fabricated rectifier's performance above 26 GHz (being significantly better than the simulated due to higher cut-off frequency), could be attributed to over-estimation of the parasitic packaging capacitance reproduced from [12], where the utilized dual-diode package results in less parasitics and hence improves the rectifier's usable frequency range. While [42] demonstrates a broadband 1 V sensitivity from 13 dBm between 14 and 23 GHz, this work is the first demonstration of a broadband 1 V sensitivity above 20 GHz, with more than 6.5 GHz of 1.2 V bandwidth from less than 12 dBm of incident power.

Table II shows a comparison of the proposed rectenna with state-of-the-art mmWave and 5G rectennas. While it can be seen that the rectennas in [7] and [41] achieve higher efficiency due to the improved single-tone impedance matching, they both have lower load impedance (reducing the voltage sensitivity) in addition to being implemented on dedicated low-loss RF substrates allowing the implementation of large-area distributed elements matching networks. On the other hand,

despite the high voltage sensitivity achieved by the 3D printed rectenna in [14], implemented on a lossy flexible 3D-printed substrate, the PCE is expected to be very low due to the high load impedance utilized to guarantee a 1 V DC output. Finally, to the best of the authors' knowledge, this is the first rectenna with a broadband 1 V sensitivity aimed at broadband mmWave 5G energy harvesting, in addition to being fabricated on textiles with a high-efficiency broadband antenna optimized for operation on-body.

B. Wearable mmWave Powering: Practical Considerations

Practical deployment of rectennas for radiative mmWave WPT and energy harvesting are dependent on the ability to deliver high power levels to the antenna. The rectenna proposed in this work, as well as in studies [7], [12], [14], require an input power in excess of 9.5 dBm to deliver a 1 V DC output across a resistive load (as compared in table II). Such a high power level may not be available as ambient radiation to be recycled from cellular communication. Therefore, it is essential to consider the applicability of such rectennas in low-cost mmWave-powered IoT applications.

In the context of harvesting energy in 5G cellular networks, the 28 GHz EIRP available from a base-station and a mobile device is 75 and 43 dBm/100 MHz, respectively [44]. Thus, given the rectenna's 7.41 dB measured realized gain, a mobile phone transmitting at 26 GHz and placed at 10 cm from the textile rectenna will result 10 dBm received power at the rectenna yielding over 1 V of DC output. Furthermore, a 1 V DC output can be achieved with more than 10 m separation between the rectenna and a mmWave base-station. 10 m is the size of a typical 10 Gbit/s 5G urban micro-cell [44]. As a result, the infrastructure (PAs and phased arrays) deployed for high-data rate 5G communications could support wireless powered networks within the network coverage. Moreover, [4] shows that a wireless-powered network operating at 28 GHz can achieve over 30 dB higher power reception for a 400 nodes/km^2 network compared to sub-6 GHz bands. However, the rectenna in our work has only evaluated the rectenna's performance under CW excitation, the impact of multi-tone modulated signals on a rectifier's performance have been previously investigated in [45].

High power mmWave power beaming has been shown to improve the power received by a rectenna at a long range (>600 m) due to the narrow beam of a directional antenna [46]. In [46], the authors study a 7 kW PA (formed of 8,192 GaN PAs with integrated power combining) which results in an 83 dBm EIRP with a 15 dB antenna. Although [46] shows that 92 GHz is the frequency where the highest power could be delivered, rectenna implementations beyond 90 GHz, such as [43], use diodes with significantly higher costs than the MA4E1319 used in this work. For example, a single Virginia Diodes W-band diode can cost $15-100, making it unsuitable for low-cost IoT applications. Moreover, to ensure compatibility of the developed antenna and rectifier with future commercial 5G applications, the choice of frequency in this work is kept below 30 and 40 GHz for the rectifier and the antenna, respectively.
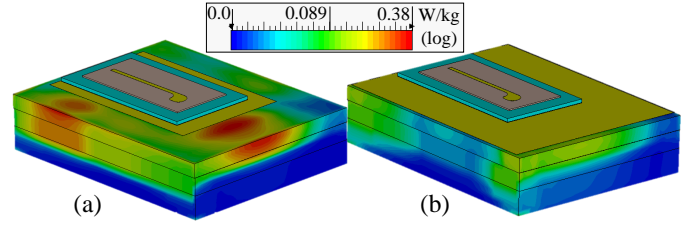

Fig. 19. Simulated SAR of the AVA at 0.1 mm from the body with: (a) a reflector covering 48% of the tissue layer, (b) a reflector covering the entire tissue layer.

In wearable operation, mmWave power beaming to on-body devices from an off-body source needs to comply with the safety regulations. In high-power directional WPT applications, multiple control and detection techniques have been proposed to ensure the high-power waves are only directed towards the rectenna to prevent "frying" an unintended target [47]. As the proposed rectenna can be used in large-area energy harvesting arrays, with DC combining as in [48], the full textile reflector backing allows additional shielding of the user.

To further investigate the interaction between the antenna and the human body, the antenna has been simulated in CST Microwave Studio over a human skin model. The uniform 4 mm-tick skin layer is based on the measured tissue dielectric properties in [49] at 28 GHz. Above 11 GHz, incident waves do not penetrate deeper than 1 mm while skin is typically 3-4 mm-thick [49]. The skin layer is placed at 0.1 mm (air gap) from the textile rectenna. A 5 mm fat and 6.7 mm muscle layer were added beneath the skin layer. The tissue model is 55×75 mm^2. Homogeneous human body models have been used to model the human tissue for both transmitting, [26], and receiving antennas [48].

Given the reciprocal nature of antennas, Specific Absoprtion Rate (SAR) analysis could be used to estimate the absorption at a certain input power level. The proposed rectenna achieves a measured PCE of 4.2%, with a DC output of 6.5 V across a 10 kΩ load, from a 20 dBm 24 GHz input. Thus, it can be assumed that the rectenna could be used to generate power at power levels higher than 20 dBm. An input power source of 0.5 W (27 dBm) is considered for the SAR analysis. Fig. 19-b shows the simulated SAR of the proposed AVA at 28 GHz. For both the compact and full-size reflectors, the peak SAR of 0.38 and 0.092 W/kg, respectively, confirm that the proposed rectenna could be used safely for wearable high-power mmWave reception while complying with the IEEE C95.1 regulations.

VI. CONCLUSION

In this paper, a textile-based broadband rectenna for 5G RF energy harvesting and WPT has been presented based on a novel wearable antenna design and a broadband high-sensitivity rectifier. The textile antenna achieves the highest radiation efficiency of reported textile-based mmWave antennas at more than 70% with a stable gain over 8 dB. The proposed rectenna is capable of generating a 1 V DC output

from 21.5 to 25 GHz from power levels as low as 9.5 dBm, more than 1.3 V from 20 to 26.5 GHz from 12 dBm of wireless power, a 15% half-power fractional bandwidth, and up to 6.5 V from 20 dBm at 24 GHz, the highest voltage compared to reported low-power mmWave rectennas. This work is the first demonstration of a textile-based rectenna operating beyond 20 GHz and the first broadband rectenna beyond for 20-26.5 GHz mmWave EH and WPT. This work demonstrates the feasibility of mmWave-powering of unobtrusive sensing and communication implemented on low-cost materials, with the capability of providing a sufficient DC output within the transmission limits of future mmWave 5G networks, as well as the safety-compliance of the proposed antenna for high-power point-to-point mmWave power transmission.

REFERENCES

[1] I. A. Hemadeh, K. Satyanarayana, M. El-Hajjar, and L. Hanzo, "Millimeter-Wave Communications: Physical Channel Models, Design Considerations, Antenna Constructions, and Link-Budget," *IEEE Communications Surveys & Tutorials*, vol. 20, 2, pp. 870 – 913, 2017.

[2] T. D. P. Perera, D. N. K. Jayakody, S. K. Sharma, S. Chatzinotas, and J. Li, "Simultaneous Wireless Information and Power Transfer (SWIPT): Recent Advances and Future Challenges," *IEEE Communication Surveys and Tutorials*, vol. 20, 1, pp. 264 – 302, 2018.

[3] A. Costanzo and D. Masotti, "Energizing 5G: Near- and Far-Field Wireless Energy and Data Trantransfer as an Enabling Technology for the 5G IoT," *IEEE Microw. Mag.*, vol. 18, no. 3, pp. 125 – 136, 2017.

[4] T. A. Khan, A. Alkhateeb, and R. W. Heath, "Millimeter Wave Energy Harvesting," *IEEE Trans. Wireless Communications*, vol. 15, 9, pp. 6048 – 6062, 2016.

[5] L. Wang, K.-K. Wong, R. W. Heath, and J. Yuan, "Wireless powered dense cellular networks: How many small cells do we need?" *IEEE Journal on Selected Areas in Communications*, vol. 35, no. 9, pp. 2010 – 2024, 2017.

[6] M. Tabesh, N. Dolatsha, A. Arbabian, and A. M. Niknejad, "A Power-Harvesting Pad-Less Millimeter-Sized Radio," *IEEE Journal of Solid-State Circuits*, vol. 50, 4, pp. 962 – 977, 2015.

[7] S. Ladan, A. B. Guntupalli, and K. Wu, "A High-Efficiency 24 GHz Rectenna Development Towards Millimeter-Wave Energy Harvesting and Wireless Power Transmission," *IEEE Trans. Circuits And Systems*, vol. 61, 12, pp. 3358 – 3366, 2014.

[8] S. Ladan and K. Wu, "Nonlinear Modeling and Harmonic Recycling of Millimeter-Wave Rectifier Circuit," *IEEE Trans. Microw. Theory Techn.*, vol. 63, 3, pp. 937 – 944, 2015.

[9] M. Nariman, F. Shirinfar, A. P. Toda, S. Pamarti, A. Rofougaran, and F. D. Flaviis, "A Compact 60-GHz Wireless Power Transfer System," *IEEE Trans. Microw. Theory Techn.*, vol. 64, no. 8, pp. 2664 – 2677, 2016.

[10] A. Collado and A. Georgiadis, "24 ghz substrate integrated waveguide (siw) rectenna for energy harvesting and wireless power transmission," in *IEEE MTT-S International Microwave Symposium Digest (MTT)*, 2013.

[11] S. Daskalakis, J. Kimionis, J. Hester, A. Collado, M. M. Tentzeris, and A. Georgiadis, "Inkjet printed 24 ghz rectenna on paper for millimeter wave identification and wireless power transfer applications," in *2017 IEEE MTT-S International Microwave Workshop Series on Advanced Materials and Processes for RF and THz Applications (IMWS-AMP)*, 2017.

[12] J. Bito, V. Palazzi, J. Hester, R. Bahr, F. Alimenti, P. Mezzanotte, L. Roselli, and M. M. Tentzeris, "Millimeter-wave ink-jet printed RF energy harvester for next generation flexible electronics," in *2017 IEEE Wireless Power Transfer Conference (WPTC)*, 2017.

[13] M. Wagih, A. S. Weddell, and S. Beeby, "Rectennas for RF Energy Harvesting and Wireless Power Transfer: a Review of Antenna Design," *IEEE Antennas and Propagation Magazine*, vol. Accepted: In Press, 2019.

[14] T.-H. Lin, S. N. Daskalakis, A. Georgiadis, and M. M. Tentzeris, "Achieving fully autonomous system-on-package designs: An embedded-on-package 5g energy harvester within 3d printed multilayer flexible packaging structures," in *2019 IEEE MTT-S International Microwave Symposium (IMS)*, 2019.

[15] A. Eid, J. Hester, and M. M. Tentzeris, "A Scalable High-Gain and Large-Beamwidth mm-Wave Harvesting Approach for 5G-powered IoT," in *2019 IEEE MTT-S International Microwave Symposium (IMS)*, 2019.

[16] Y. Rajavi, M. Taghivand, K. Aggarwal, A. Ma, and A. S. Y. Poon, "An rf-powered fdd radio for neural microimplants," *IEEE Journal of Solid-State Circuits*, vol. 52, no. 5, pp. 1221 – 1229, 2017.

[17] S. Yang, J. Yin, H. Yi, W.-H. Yu, P.-I. Mak, and R. P. Martins, "A 0.2-V Energy-Harvesting BLE Transmitter With a Micropower Manager Achieving 25% System Efficiency at 0-dBm Output and 5.2-nW Sleep Power in 28-nm CMOS," *IEEE Journal of Solid-State Circuits*, vol. 54, no. 5, pp. 1351 – 1362, 2019.

[18] M. Taghivand, K. Aggarwal, Y. Rajavi, and A. S. Y. Poon, "An Energy Harvesting 2x2 60 GHz Transceiver With Scalable Data Rate of 38=2450 Mb/s for Near-Range Communication," *IEEE Journal of Solid State Circuits*, vol. 50, 8, pp. 1889 – 1902, 2015.

[19] M. Wagih, A. S. Weddell, and S. Beeby, "Millimeter-Wave Textile Antenna for On-Body RF Energy Harvesting in Future 5G Networks," in *2019 IEEE Wireless Power Transfer Conference (WPTC)*, 2019.

[20] 5G Spectrum Positions. [Online]. Available: www.gsma.com/spectrum/wp-content/uploads/2019/02/5G-Spectrum-Positions-InfoG.pdf

[21] M. Moosazadeh, S. Kharkovsky, J. T. Case, and B. Samali, "Improved Radiation Characteristics of Small Antipodal Vivaldi Antenna for Microwave and Millimeter-Wave Imaging Applications," *IEEE Antennas Wireless Propag. Lett.*, vol. 16, pp. 1961 – 1964, 2017.

[22] S.-E. Adami, P. Proynov, G. S. Hilton, G. Yang, C. Zhang, D. Zhu, Y. Li, S. P. Beeby, I. J. Craddock, and B. H. Stark, "A Flexible 2.45-GHz Power Harvesting Wristband With Net System Output From -24.3 dBm of RF Power," *IEEE Trans. Microw. Theory Techn.*, vol. 66, 1, pp. 380–395, 2018.

[23] N. Chahat, M. Zhadobov, S. A. Muhammad, L. L. Coq, and R. Sauleau, "60-GHz Textile Antenna Array for Body-Centric Communications," *IEEE Trans. Antennas Propag.*, vol. 61, 4, pp. 1816 – 1824, 2013.

[24] B. S. Cook, B. Tehrani, J. R. Cooper, and M. M. Tentzeris, "Multilayer Inkjet Printing of Millimeter-Wave Proximity-Fed Patch Arrays on Flexible Substrates," *IEEE Antennas Wireless Propag. Lett.*, vol. 12, pp. 1351 – 1354, 2013.

[25] H. R. Khaleel, "Design and Fabrication of Compact Inkjet Printed Antennas for Integration Within Flexible and Wearable Electronics," *IEEE Trans. Components, Packaging and Manufacturing Technology*, vol. 4, no. 10, pp. 1722 – 1728, 2014.

[26] M. Wagih, Y. Wei, and S. Beeby, "Flexible 2.4 GHz Sensor Node for Body Area Networks with a Compact High-Gain Planar Antenna," *IEEE Antennas Wireless Propag. Lett.*, vol. 17, 12, pp. 49 – 53, 2018.

[27] A. Dierck, H. Rogier, and F. Declercq, "A Wearable Active Antenna for Global Positioning System and Satellite Phone," *IEEE Trans. Antennas Propag.*, vol. 61, no. 2, pp. 532 – 538, 2013.

[28] A. Kiourti, C. Lee, and J. L. Volakis, "Fabrication of Textile Antennas and Circuits With 0.1 mm Precision," *IEEE Antennas Wireless Propag. Lett.*, vol. 15, pp. 151 – 153, 2016.

[29] N. Chahat, M. Zhadobov, L. L. Coq, S. I. Alekseev, and R. Sauleau, "Characterization of the Interactions Between a 60-GHz Antenna and the Human Body in an Off-Body Scenario," *IEEE Trans. Antennas Propag.*, vol. 60, 12, pp. 5958 – 5965, 2012.

[30] A. Komolafe, Y. Torah, Russel ans Wei, H. Nunesmatos, M. Li, D. Hardy, T. Dias, M. Tudor, and S. Beeby, "Integrating flexible filament circuits for etextile applications," *Advanced Materials Technologies*, vol. 4, no. 7, 2019.

[31] M.-Q. Lee and S. Nam, "An accurate broadband measurement of substrate dielectric constant," *IEEE Microwave and Guided Wave Letters*, vol. 6, 4, pp. 168 – 170, 1996.

[32] A. R. Guraliuc, M. Zhadobov, O. D. Sagazan, and R. Sauleau, "Solid Phantom for Body-Centric Propagation Measurements at 60 GHz," *IEEE Trans. Microw. Theory Techn.*, vol. 62, 6, pp. 1373 – 1380, 2014.

[33] S. F. Jilani, M. O. Munoz, Q. H. Abbasi, and A. Alomainy, "Millimeter-Wave Liquid Crystal Polymer Based Conformal Antenna Array for 5G Applications," *IEEE Antennas Wireless Propag. Lett.*, vol. 18, 1, pp. 84, 88, 2019.

[34] N. Chahat, M. Zhadobov, L. L. Coq, and R. Sauleau, "Wearable Endfire Textile Antenna for On-Body Communications at 60 GHz," *IEEE Antennas Wireless Propag. Lett.*, vol. 11, pp. 799 – 802, 2012.

[35] J. Semple, D. G. Georgiadou, G. Wyatt-Moon1, G. Gelinck, and T. D. Anthopoulos, "Flexible diodes for radio frequency (RF) electronics: a materials perspective," *Semiconductor Science and Technology*, vol. 32, 2017.

[36] M. K. Matters-Kammerer, L. Tripodi, R. van Langevelde, J. Cumana, and R. H. Jansen, "RF Characterization of Schottky Diodes in 65-nm CMOS," *IEEE Trans. Electron Devices*, vol. 57 no. 5, pp. 1063 – 1068, 2010.

[37] S. Hemour, Y. Zhao, C. H. P. Lorenz, D. Houssameddine, Y. Gui, C.-M. Hu, and K. Wu, "Towards Low-Power High-Efficiency RF and Microwave Energy Harvesting," *IEEE Trans. Microw. Theory Techn.*, vol. 62 no. 4, pp. 965 – 976, 2014.

[38] S. Ladan, S. Hemour, and K. Wu, "Towards Millimeter-Wave High-Efficiency Rectification for Wireless Energy Harvesting," in *2013 IEEE International Wireless Symposium (IWS)*, 2013.

[39] J. Kimionis, A. Collado, M. M. Tentzeris, and A. Georgiadis, "Octave and Decade Printed UWB Rectifiers Based on Nonuniform Transmission Lines for Energy Harvesting," *IEEE Trans. Microw. Theory Techn.*, vol. 65, no. 11, pp. 4326 – 4334, 2017.

[40] C. H. P. Lorenz, S. Hemour, and K. Wu, "Physical Mechanism and Theoretical Foundation of Ambient RF Power Harvesting Using Zero-Bias Diodes," *IEEE Trans. Microw. Theory Techn.*, vol. 64 no. 7, pp. 2146 – 2158, 2016.

[41] A. Mavaddat, S. H. M. Armaki, and A. R. Erfanian, "Millimeter-Wave Energy Harvesting Using 4x4 Microstrip Patch Antenna Array," *IEEE Antennas Wireless Propag. Lett.*, vol. 14, pp. 515 – 518, 2014.

[42] A. Takacs, H. Aubert, S. Fredon, L. Despoisse, and H. Blondeaux, "Microwave Power Harvesting for Satellite Health Monitoring," *IEEE Trans. Microw. Theory Techn.*, vol. 62, 4, pp. 1090–1098, 2014.

[43] S. Hemour, C. H. P. Lorenz, and K. Wu, "Small-footprint wideband 94 GHz rectifier for swarm micro-robotics," in *2015 IEEE MTT-S International Microwave Symposium*, 2015.

[44] Y. Huo, X. Dong, and W. Xu, "5g cellular user equipment: From theory to practical hardware design," *IEEE Access*, vol. 5, 2017.

[45] F. Bolos, J. Blanco, A. Collado, and A. Georgiadis, "RF Energy Harvesting From Multi-Tone and Digitally Modulated Signals," *IEEE Trans. Microw. Theory Techn.*, vol. 64, no. 6, pp. 1918 – 1927, 2016.

[46] H. Kazemi, K. Shinohara, and C. W. Eckhardt, "Millimeter Wave Wireless Power Transmission-Technologies and Applications," in *IEEE Wireless Power Transfer Conference*, 2019.

[47] R. M. Dickinson, "Power in the sky: Requirements for microwave wireless power beamers for powering high-altitude platforms," *IEEE Microw. Mag.*, vol. 14 no. 2, pp. 36 – 47, 2013.

[48] D. Vital, S. Bhardwaj, and J. L. Volakis, "Textile Based Large Area RF-Power Harvesting System for Wearable Applications," *IEEE Trans. Antennas Propag.*, vol. Early Access, 2019.

[49] D. Ghodgaonkar, O. Gandhi, and M. Iskander, "Complex permittivity of human skin in vivo in the frequency band 26.5-60 GHz," in *IEEE Antennas and Propagation Society International Symposium*, 2000.

Geoffrey S. Hilton received the B.Sc. degree from the University of Leeds, Leeds, U.K., in 1984, and the Ph.D. degree from the University of Bristol, Bristol, U.K., in 1993, for research on the design and finite-difference time-domain modeling of printed antenna elements.

He is a Senior Lecturer with the University of Bristol. His current research interests include practical antenna and system design for a variety of communications and radar applications such as ground penetrating radar, performance evaluation of antennas in mobile radio, electrically small elements, active/tuneable elements, and vehicle-mounted conformal antennas.

Alex S. Weddell (GS'06-M'10) received the M.Eng. degree (1st class honors) and Ph.D. in electronic engineering from the University of Southampton, U.K., in 2005 and 2010.

His main research focus is in the areas of energy harvesting and energy management for future Internet of Things devices. He has over 14 years experience in design and deployment of energy harvesting systems, and has published around 55 peer-reviewed papers in the area. He is currently a Lecturer in the Center for Internet of Things and Pervasive Systems at the University of Southampton, and is involved with three projects funded by EPSRC, EU Horizon 2020 and Clean Sky 2.

Mahmoud Wagih (GS'18) received his B.Eng. (Hons.) from the University of Southampton in 2018, where he is currently pursuing his Ph.D.

In 2017 he worked as a Research Assistant at the University of Southampton, supported by Intel, investigating novel differential transmission lines. In 2018, he was a Hardware Engineering Intern at Arm, UK, and, in 2020, a devices research intern at Arm,. His current research interests lie in RF energy harvesting, wireless power transfer, and mmWave wearable antennas. He has over 20 journal and conference publications in these areas.

Mr. Wagih is a graduate student member of the IEEE. He was the recipient of the Best Undergraduate Project Prize at the University of Southampton, 2018, and was selected for the IEEE MTT-S International Microwave Symposium Project Connect, 2019. He is the recipient of the Best Student Paper Award at the IEEE MTT-S Wireless Power Transfer Conference, 2019, and the Best Oral Paper at PowerMEMS 2019.

Steve Beeby received the B.Eng. (Hons.) degree in mechanical engineering from the University of Portsmouth, Portsmouth, U.K., in 1992, and the Ph.D. degree in MEMS resonant sensors from the University of Southampton, Southampton, U.K., in 1998.

He is currently the Head of the Smart Electronic Materials and Systems Research Group and leads the U.K.'s E-Textiles Network. He is currently leading three U.K. funded research projects and has received over 16 million research funding. He is a Co-Founder of Perpetuum Ltd., a University spin-out based upon vibration energy harvesting formed in 2004, Smart Fabric Inks Ltd., and D4 Technology Ltd. He has co-authored/edited four books including Energy Harvesting for Autonomous Systems (Artech House, 2010). He has given 25 invited talks and has over 300 publications and 10 patents. He has an h-Index of 52. His current research interests focus on energy harvesting, e-textiles and the use of energy harvesting in wearable applications.

Dr. Beeby was the recipient of two prestigious EPSRC Research Fellowships to investigate the combination of screen-printed active materials with micromachined structures and textiles for energy harvesting and was also awarded a Personal Chair in 2011. He is currently the Chair of the International Steering Committee for the PowerMEMS Conference series.